Asian Journal of Pharmaceutical Sciences 21 (2026) 101128

Available online at www.sciencedirect.com

ScienceDirect

journal homepage: www.elsevier.com/locate/AJPS



Research Article

Freezing shock monocytes deliver antisense oligonucleotides via liposomes for the treatment of idiopathic pulmonary fibrosis

Hailong Li[a,1], *Xi Wu*[a,1], *Jinhe Li*[a], *Liqing Han*[a], *Hongting Liu*[a], *Qiuyan Jiang*[a], *Bowen Liu*[a], *Qin Xia*[a], *Zherui Li*[a], *Xiaohe Li*[a], *Songtao Gu*[c], *Aiguo Xu*[d], *Honggang Zhou*[a], *Xiaoting Gu*[a,*], *Zuojun Xu*[b,*], *Xiaoyu Ai*[a,*], *Cheng Yang*[a,*]

[a] *The State Key Laboratory of Medicinal Chemical Biology, College of Pharmacy and Key Laboratory of Molecular Drug Research, Nankai University, Tianjin 300350, China*

[b] *Department of Respiratory and Critical Care Medicine, Peking Union Medical College Hospital, Chinese Academy of Medical Sciences and Peking Union Medical College, Beijing 100730, China*

[c] *Department of Respiratory & Critical Care Medicine, Tianjin Chest Hospital, Tianjin 300222, China*

[d] *Department of Respiratory and Critical Care Medicine, The First Affiliated Hospital of Zhengzhou University, Zhengzhou 450000, China*

ARTICLE INFO

Article history:
Received 3 June 2025
Revised 23 September 2025
Accepted 28 December 2025
Available online 24 January 2026

Keywords:
Connective tissue growth factor
Idiopathic pulmonary fibrosis
Antisense oligonucleotides
Nintedanib
Matrix metalloproteinase 2
Lung function

ABSTRACT

Connective tissue growth factor (CTGF) is a key driver in the pathogenesis of idiopathic pulmonary fibrosis (IPF). This study presents a groundbreaking supramolecular cryo-shock bone marrow mononuclear cell system for targeted drug delivery in IPF. We incorporated antisense oligonucleotides (ASO) to inhibit CTGF and simultaneously encapsulated nintedanib using the ZMO-E5-NPs carrier for synergistic delivery. The cryo-shock treatment enhances cellular structural integrity and preserves receptor functionality, thereby extending cell viability. By modifying the E5 peptide and conjugating it with DSPE-PEG-MAL, we developed a composite carrier, ZMO-E5-NPs, which demonstrates efficient lung-targeting capability. This system enables rapid nanoparticle capture by fibroblasts through matrix metalloproteinase 2 (MMP2) recognition, ensuring precise delivery of both ASO and nintedanib. In a bleomycin-induced pulmonary fibrosis mouse model, ZMO-E5-NPs-ASO (nintedanib-containing group) significantly attenuated fibrosis progression, improved lung function, and exhibited excellent biocompatibility and safety, highlighting its potential as a novel therapeutic strategy for respiratory diseases.

© 2026 Published by Elsevier B.V. on behalf of Shenyang Pharmaceutical University.
This is an open access article under the CC BY-NC-ND license
(http://creativecommons.org/licenses/by-nc-nd/4.0/)

* Corresponding authors.
E-mail addresses: guxiaoting@nankai.edu.cn (X. Gu), xuzj@hotmail.com (Z. Xu), aixiaoyu@nankai.edu.cn (X. Ai), yangcheng@nankai.edu.cn (C. Yang).

[1] These authors contributed equally to this work

Peer review under responsibility of Shenyang Pharmaceutical University.

https://doi.org/10.1016/j.ajps.2026.101128

1818-0876/© 2026 Published by Elsevier B.V. on behalf of Shenyang Pharmaceutical University. This is an open access article under the CC BY-NC-ND license (http://creativecommons.org/licenses/by-nc-nd/4.0/)

1. Introduction

Idiopathic pulmonary fibrosis (IPF) is a chronic and progressive lung disease characterized by an increase in fibrotic tissue and impaired lung function [1]. The etiology of IPF is unknown, and there is a lack of effective treatment options, leading to poor prognosis, with a median survival time from diagnosis to death of about 3–5 years [2]. Pirfenidone and nintedanib are the only drugs approved for the treatment of IPF, but they only help to slow the progression of fibrosis and are not curative therapies [3,4]. Clinical studies have shown that patients infected with the COVID-19 disease may exhibit fibrotic responses to some extent [5,6]. Therefore, there is an urgent need to explore treatable targets and develop new therapeutic methods to slow down or even reverse the progression of IPF.

Activation of lung tissue damage repair program recruits a large number of inflammatory cells and fibroblasts [7]. Fibroblasts differentiate into myofibroblasts and secrete collagen and extracellular matrix to promote IPF [8]. Fibroblasts secrete a large number of cytokines during differentiation, and there is a lot of evidence that the expression of pro-fibrotic mediators such as connective tissue growth factor (CTGF) is increased and activated, leading to the recruitment and activation of fibroblasts [9,10]. In recent years, research on the potential of CTGF in disease treatment has been increasing and has received more attention. Several drugs targeting CTGF are being evaluated through clinical or preclinical trials, especially showing promising results in pulmonary fibrosis [11]. CTGF has become a potential target for drug development for the treatment of IPF [12]. Oligonucleotides are nucleic acid polymers that have the potential to treat or manage a variety of diseases [13]. Oligonucleotides can regulate gene expression through a series of processes mediated by RNAi and RNaseH, including target degradation, splicing regulation, non-coding RNA inhibition and gene activation [14]. Antisense oligonucleotides (ASO) can regulate the expression of pathogenic genes from the root and solve some targets that are difficult to develop drugs. Compared with small molecule and monoclonal antibody, ASO drugs have the advantages of abundant targets, long half-life, high safety and high success rate in clinical development [15,16]. At present, a total of 10 ASO drugs have been approved for market, and >50 ASO drugs are in the clinical research stage. Despite recent technological advances, however, there are still many challenges that hinder the clinical application of ASOs, including its degradation or degeneration in the blood and low delivery efficiency. Therefore, effective and biocompatible vectors are needed to overcome the ASO targeting problem.

In previous studies, Li et al. used liquid nitrogen to efficiently prepare dead cells on the basis of cell bionic delivery system, and obtained dead cells with complete cell structure but no proliferative ability [17]. Xu et al. treated acute pneumonia with targeted drug delivery of rapid freezing macrophages [18]. The development of low temperature shock cells provides a new solution for the development of cell bionic delivery systems [19]. The above studies have developed new ideas and directions for the development of ASO drug delivery systems. Here, we have developed a supramolecular cryo-shock bone marrow mononuclear cell "hitchhiking" drug delivery system. After cryogenic freezing of mononuclear cells, they are connected with engineered liposomes loaded with CTGF ASO and modified with matrix metalloproteinase 2 (MMP2) responsive peptide (E5), combined with nintedanib and ASO, so that the drug is encapsulated while having inflammatory tropism, and is applied to the treatment of pulmonary fibrosis (Fig. 1). Monocytes are members of the mononuclear phagocyte system (MPS), originating from hematopoietic stem cells in the bone marrow and developing in the bone marrow [20,21]. Their main biological processes in the body are the ability to phagocytize foreign bodies and present antigens, migrate to sites of injury and inflammation, and have inflammatory tropism [21]. Peptide E5 is a straight chain composed of amino acid residues, whose main structural characteristic is the presence of two MMP-2 specific cleavage sequences, while also being able to target the chemokine receptor 4 (CXCR4) [22]. The frozen monocyte-peptide E5 nanoparticles drug delivery system developed in this study is of great significance for the treatment of idiopathic pulmonary fibrosis, and provides a new solution for the transformation and upgrading of cell bionic delivery system.

2. Materials and methods

2.1. *Materials*

1,2-distearoyl-sn-glycero-3-phosphoethanolamine-N-[methoxy(polyethylene glycol)-2000] (DSPE-PEG-MAL, MW = 2000 Da) was purchased from Yuanye Biological Technology Co., Ltd. (Shanghai, China), and cholesterol was from Aladdin Biochemical Technology Co., Ltd. (Shanghai, China). Peptide E5 was from Nanjing Peptide Biotech Co., Ltd. (Nanjing, China). Cy7.5 was from MedChemExpress. FITC dye was from Beijing Boyuotuo Technology Co., Ltd. (Beijing, China). 1,1-dioctadecyl-3,3,3,3-tetramethylindocarbocyanine perchlorate (DiI) was from Shanghai Jizhi Biochemical Technology Co., Ltd. (Shanghai, China). Lipopolysaccharide (LPS) and carrageenan were from Solarbio (Beijing, China). Nintedanib was from Shanghai McKinley Biochemical Technology Co., Ltd. (Shanghai, China). NIH 3T3, RAW264.7 cells were from Wuhan Pronova Life Science Co., Ltd. (Wuhan, China). Antibodies against CXCR4, CXCR5 and CD47 (R380981, R24019, R380870) were from zenbio (Chengdu,China). Antibodies against Tublin, CTGF, α-smooth muscle actin (α-SMA) and Collagen I (Col-1) (RM8637, BD-PT5991, BD-PT5120, RM8542) were from Biodragon (Suzhou, China). Reverse transcription kits, reagents for RT-qPCR were from Yeasen (Cat No.11201ES08; Cat No.11151ES60; Shanghai, China). DMEM medium was from Yocon Biotechnology (Beijing) Co., Ltd. (Beijing, China). Lipo8000^{TM} transfection reagent, BCA protein concentration assay kit, cytoplasmic and membrane protein extraction kit were from Shanghai Biyuntian Biotechnology Co., Ltd. (Shanghai, China). CCK-8 cell proliferation and cytotoxicity assay kit was from Biosharp Labgic Technology Co., Ltd. (Beijing, China). Human Lung Fibroblasts cells (HLF) cells were derived from lung tissue

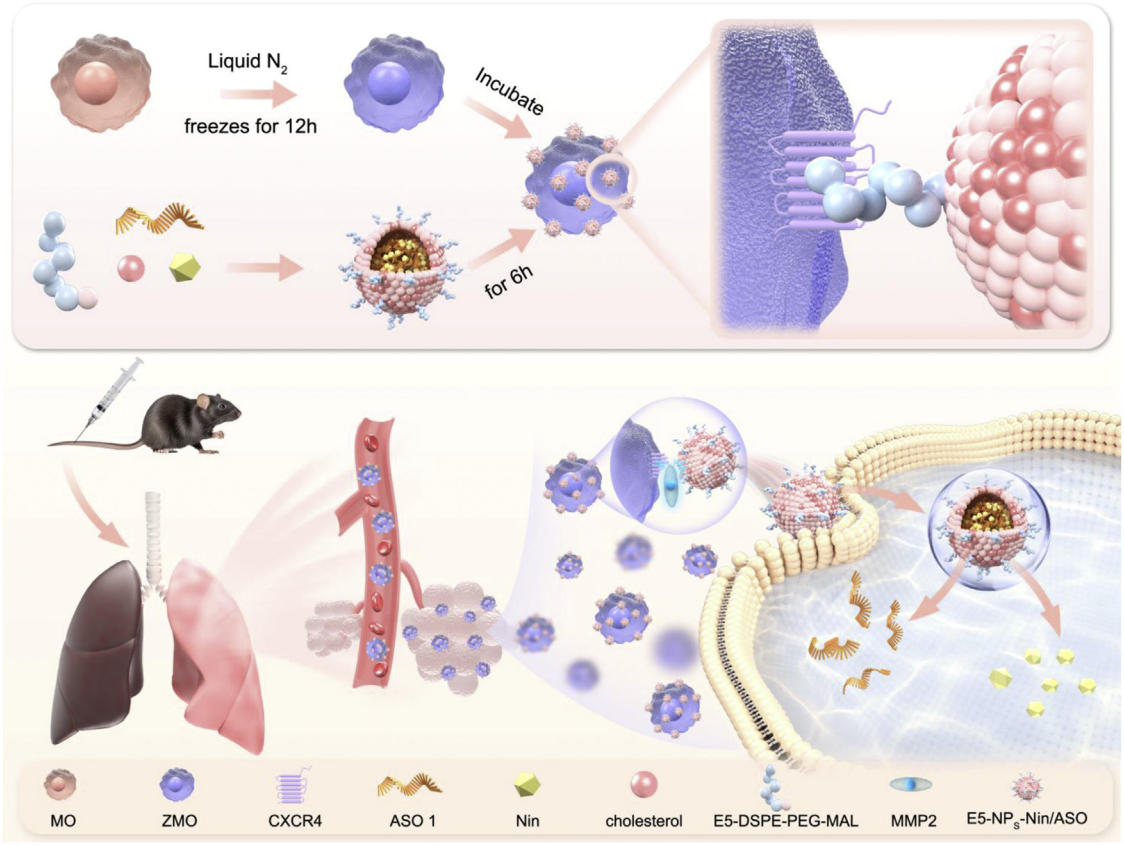


Fig. 1 – Schematic of the supramolecular cryo-shocked mononuclear cell "Hitchhiking" drug delivery system. Mononuclear cells (MO) are extracted from mouse bone marrow and subjected to cryo-shock by freezing in liquid nitrogen for 12 h, then resuspended in PBS to obtain cryo-shocked mononuclear cells (ZMO). Peptide E5 is conjugated with DSPE-PEG-MAL and self-assembles into E5-NPs. ZMO is then co-incubated with E5-NPs loaded with Nin or ASO for 4 h, forming a complex through the binding of the CXCR4 receptor, resulting in ZMO-E5-NPs-Nin/ASO. The E5-NPs-Nin/ASO, hitchhiking on ZMO, are effectively delivered to lung tissue in the form of ZMO-E5-NPs-Nin/ASO. In IPF tissue, the overexpressed MMP2 recognizes the binding site of peptide E5, causing the ZMO-E5-NPs-Nin/ASO to dissociate, and the lung fibroblasts endocytose E5-NPs-Nin/ASO, achieving an increased drug concentration in IPF tissue.

of patients with pulmonary fibrosis. Mononuclear cells (MO) were extracted from the bone marrow of C57BL/6 J mice. NIH-3T3 was purchased from ATCC. MO and NIH-3T3, RAW264.7 cells were cultured in DMEM containing 10% heat-inactivated fetal bovine serum (FBS), penicillin (100 U/ml), and streptomycin (100 μg/ml) at 37 °C, 5% CO_2 in a humidified incubator. Cell culture dishes and related products were purchased from NEST Biotechnology Co. Ltd. (Wuxi, China). RIPA (Beyotime Institute of Biotechnology) buffer with phenylmethylsulfonyl fluoride (Solarbio Science & Technology Co., Ltd, Beijing, China). The BCA assay kit (Beyotime Institute of Biotechnology) 4,6-diamidino-2-phenylindole (DAPI, Abcam, Cambridge, UK).

2.2. *Preparation and characterization of ZMO*

MOs extracted were cultured in DMEM containing 10% heat-inactivated FBS, penicillin (100 U/ml) and streptomycin (100 μg/ml) at 37 °C, 5% CO_2 in a humidified incubator for 24 h. Afterward, cells were centrifuged at 1000 rpm for 3 min to obtain a cell pellet. The cryopreservation solution was prepared at a ratio of FBS:DMSO = 9:1. The cell pellet was resuspended in 1 ml cryopreservation solution and frozen in liquid nitrogen for 12 h, then rapidly oscillated in a 37 °C water bath to thaw, and centrifuged at 1000 rpm for 3 min to obtain the cell pellet, which was resuspended in 1 mL sterile PBS to obtain Zombie mononuclear cells (ZMO).

The morphology and size of MO and ZMO were observed using a scanning electron microscope (TEM) at 200 kV (JEOL, JEM-2100F, Japan). ZMO and MO were inoculated in 96-well plates to measure cell proliferation at 0 d, 1 d and 2 d; ZMO and MO were inoculated in six-well plates to observe the integrity of cells at 0 d, 14 d and 28 d The nuclei and cell membranes of ZMO and MO were stained with Hoechst 33342 and PI dyes, respectively. The samples were photographed using a Leica TCS SP8 STED confocal microscope, and the fluorescence intensity was analyzed by flow cytometry. Membrane proteins of ZMO and MO were extracted and compared for total protein and characteristic protein content on the cell membrane surface.

2.3. Preparation of E5-DSPE-PEG-MAL

According to the literature, we synthesized a peptide E5 with the sequence GPLGIAGQ and added a cysteine at the C-terminus to become GPLGIAGQ-Cys. Subsequently, we connected the peptide to the phospholipid through an addition reaction between the thiol (-SH) group in DSPE-PEG-MAL and maleimide (MAL). Specifically, 1 mg DSPE-PEG-MAL and 500 mg GPLGIAGQ-Cys were added to DMSO and reacted at 60 °C for 24 h. Then, the reaction solution was dialyzed in a dialysis bag with a molecular weight cutoff of 2000 Da for 24 h. After dialysis, the liquid in the bag was lyophilized to obtain E5-DSPE-PEG-MAL.

2.4. Preparation and drug encapsulation of E5-NPs

In a 50 ml round-bottom flask, 20 mg DSPE-PEG-MAL-E5 and 2.7 mg cholesterol were dissolved in 4 mL methanol. The mixture was then rotary evaporated at 40 °C and 0.5 MPa for 20 min. About 4 ml deionized water was added, and the mixture was hydrolyzed at atmospheric pressure at 40 °C for 10 min. The E5-NPs were obtained by filtering through a 0.8 μm filter membrane. For the preparation of FITC-E5-NPs, E5-DSPE-PEG was replaced with FITC-E5-DSPE-PEG, with the other conditions remaining unchanged. The preparation process for E5-NPs-Nin was the same. Similarly, for E5-NPs-ASO, 4 mL pre-warmed ddH_2O containing 0.5 mg LNA-CTGF ASO was added during the hydration process, with the rest of the process remaining unchanged.

2.5. Determination of encapsulation efficiency and characterization

Encapsulation efficiency (EE) of nintedanib was determined by measuring the absorbance of nintedanib at 407 nm at different concentration gradients using a UV–Vis spectrophotometer, and a standard curve of nintedanib was established. 50 μl E5-Nin sonicated for 30 min was added to 2.5 ml methanol, and the absorbance at 407 nm was measured. EE of nintedanib is as follows: EE (%) = $(W_1/W_2) \times 100\%$, where W_1 represents the mass of encapsulated drug, and W_2 represents the mass of the entire drug. EE of ASO: E5-ASO solution was centrifuged at 4 °C, 13,000 rpm for 30 min, the supernatant was taken, and the concentration of free ASO was determined using a Nanodrop. EE (%) = (Total ASO dosage - the mass of free ASO) / Total ASO dosage × 100%.

The particle size and zeta potential of E5-Nin and E5-ASO were measured using Malvern Zetasizer ZS90 (Malvern, Nano ZS 90, U.K.).

2.6. Preparation and characterization of MO-E5-NPs and ZMO-E5-NPs

MO and ZMO were mixed with E5-NPs in a flask at a certain ratio, incubated at 37 °C, 100 rpm for 4 h, centrifuged at 1000 rpm for 3 min, and the pellet was taken, resuspended in sterile PBS. Dil dye (10 μg/ml) was added to ZMO and MO, incubated at 37°C in the dark for 15 min, centrifuged at 400 g for 3 min, washed twice with PBS, resuspended in 1 mL PBS, and 10 μg/mL Hoechst 33342 was added, incubated at 37 °C in the dark for 20 min, centrifuged at 400 g for 3 min, washed twice with PBS, resuspended in 1 ml PBS. Then, the stained ZMO and MO were incubated with FITC-E5-NPs at 37°C, with incubation times of 1 h, 2 h and 4 h. Photographed using a Leica TCS SP8 STED confocal microscope.

2.7. ZMO-E5-NPs inflammation homing verification

Male C57BL/6 J mice were randomly divided into six groups ($n = 3$). The right hind paw was injected with 20 μL 3% (w/v) carrageenan to establish a mouse foot edema model. About 4 h after injection, each mouse was tail vein injected with 100 μL Cy7.5, E5-Cy7.5-NPs or ZMO–Cy7.5-E5-NPs according to the group. The mice were imaged using the IVIS (Lumina XR III) for *in vivo* imaging and biodistribution analysis1 h after injection, with an excitation wavelength of 549 ± 20 nm and an emission wavelength of 565 ± 20 nm. bleomycin (Bleomycin)-Induced IPF Model: Male C57BL/6 J mice were randomly divided into six groups ($n = 3$). Each mouse was given a single intratracheal instillation of BLM at a concentration of 2U/kg. On the 7 d after instillation, each mouse was tail vein injected with 100 μl Cy7.5, E5-Cy7.5-NPs or ZMO–Cy7.5-E5-NPs according to the group. About 8 h after injection, the mice were imaged using the IVIS (Lumina XR III) for *in vivo* and *ex vivo* biodistribution analysis, with an excitation wavelength of 788 nm and an emission wavelength of 808 nm.

2.8. ASO drug design and modification

ASO Sequence: TATGTCTTCATGCTGGTGCAG, a total of 21 bases. Full-chain phosphorothioate, with the first six bases at the 5 end and the last six bases at the 3 end modified by LNA-modified RNA bases, that is, the 2-O and 4-C atoms on the ribose are connected by different condensation to form a methylene bridge and form a ring, with the middle 11 bases being DNA; ASO negative control and ASO purchased from Qingke Bio (Beijing, China).

2.9. Cell transfection

Lipofectamine 8000 was used for cell transfection according to the manufacturer's instructions. Specifically, mononuclear cells were grown to 80% on a six-well culture plate. After discarding the medium, the cells were washed twice with sterile PBS. ASO or negative control was mixed with Lipofectamine transfection reagent at the ratio indicated in the instructions and transfected into the cells. About 6 h later, the supernatant was discarded, and fresh medium containing 20% FBS was added.

2.10. RNA extraction and qRT-PCR

All samples were extracted by TRIzol reagent (Invitrogen; Thermo Fisher Scientific, Inc., Waltham, MA, USA), and total RNA was isolated according to the manufacturer's instructions. The YEASEN reverse transcription kit was used to transcribe RNA into cDNA, containing the following in a 20 μl reaction mixture: total RNA (1 μg), RT enzyme primer (2 μl), 5 × *g* DNA digester Mix (3 μl), 4 × Hifair III SuperMix plus (5 μl), RNase-free H_2O (to a total volume of 20 μl). The RT reaction

Table 1 – Primer sequence.

Gene	Forward (5′–3′)	Return (5′–3′)
GAPDH	TGGATTTGGACGCATTGGTC	TTTGCACTGGTACGTGTTGA
Col1a1	CCAAGAAGACATCCCTGAAGTCA	TGCACGTCATCGCACACA
α-SMA	GCTGGTGATGATGCTCCCA	GCCCATTCCAACCATTACTCC
CTGF	AGAACTGTGTACGGAGCGTG	GTGCACCATCTTTGGCAGTG
TNF-α	GACGTGGAACTGGCAGAAGAG	TTGGTGGTTTGTGAGTGTGAG
IL-6	TAGTCCTTCCTACCCCAATTTCC	TTGGTCCTTAGCCACTCCTTC
IL-1β	AGCTTCAGGCAGGCAGTATC	AAGGTCCACGGGAAAGACAC
Fn	AAGGATGGAGTGATAGCAACCC	TCTGCTTGAAATCTGGTGTGC

was carried out as follows: 55 °C for 15 min, 85 °C for 5 min. Quantitative Real-Time Polymerase Chain Reaction (qRT-PCR) was performed using Fast SYBR Green Chemistry (TaKaRa, Japan). Primers are shown in Table 1. Real-time fluorescence quantitative PCR was performed in triplicate on the CFX96 Real-Time Fluorescence Quantitative PCR Detection System (Bio-Rad, West Berkeley, CA). The relative gene expression was determined by the $2^{-\Delta\Delta CT}$ method, normalizing mature miRNA to GAPDH.

2.11. Cell viability

Cell viability was determined by the Cell Counting Kit-8 (CCK-8; Biosharp Labgic Technology Co., Ltd.). Lung fibroblast cells were cultured in a 96-well plate to a density of 70%. Different concentrations of LNA-CTGF ASO, nintedanib, ZMO-E5-Nin, ZMO-E5-ASO were added, and the cells were incubated with the cells at 37 °C and 5% CO_2 for 24 h. Then, the supernatant was discarded, each well was washed with PBS, and 10 µl CCK-8 reagent was added to each cell well. The cells were incubated in the dark at 37 °C for 2 h, and the absorbance at 450 nm was measured.

2.12. Protein blotting

Total protein was extracted from cells. Cells were lysed in RIPAbuffer with phenylmethylsulfonyl fluoride. The BCA assay kit was then used to measure protein concentration. Total protein samples were loaded onto 8%–12% SDS-polyacrylamide gels, and separated proteins were transferred onto PVDF membranes. The membranes were incubated with primary antibodies (CXCR4, CXCR5, CD47, α-SMA, Col-1, CTGF, 1:1000) overnight at 4°C, then incubated with secondary antibodies (1:10,000) for 2 h. Finally, the blots were scanned using the Tanon 5200 Multifunctional Imaging System.

2.13. Cell migration assay

NIH-3T3 cells were seeded in a six-well plate to 80%−100% density, then serum-starved, and a 100 µm wound was created by scraping with a 200 µl sterile pipette tip. The cells were then treated with TGF-β1, Nin and ASO according to the group. The wound was photographed at 0 h, 12 h, 24 h and 48 h using an optical microscope (Nikon, Japan). Distance (ratio to 0 h) = Percentage of the wound at 12 h, 24 h and 48 h/Data at 0 h.

2.14. In vitro drug release study

The dialysis method was used to study the Nin drug release from E5-NPs and ZMO-E5-NPs. E5-NP or ZMO-E5-NP (1.0 ml, equivalent to 100 µg/ml of Nin) solution was transferred to a dialysis bag (MW = 1000 Da) and immersed in 29 ml PBS (containing 5% Tween-20, v/v), with or without the supernatant of RAW 264.7 cells stimulated with 2 µg/ml LPS. The dialysis system was continuously shaken at 37 °C (100 rpm). At the designated times, 1 ml dialysis solution was taken for measurement and replaced with 1 mL fresh dialysis medium. The content of released Nin was measured at 407 nm using a UV–Vis spectrophotometer (Beckman Coulter, DU730, USA). The cumulative release percentage of Nin was calculated and described as the mean ± standard deviation (SD) of the repeats, and the cumulative release curve was plotted.

2.15. In vitro cellular uptake

The early stage of IPF is characterized by severe inflammation, and the later stage is a coexistence of inflammation and fibrosis. Frozen mononuclear cells mainly have the characteristic of inflammatory homing, so LPS-induced inflammatory macrophages and primary lung fibroblast cells from patients were chosen as *in vitro* models. RAW 264.7 cells and primary lung fibroblast cells from patients were seeded in a confocal dish at a density of 5×10^5 cells/well and cultured overnight at 37 °C (5% CO_2). After that, RAW 264.7 cells were stimulated with 2 µg/ml LPS for 24 h to obtain inflammatory RAW 264.7 cells. Then, FITC-E5-NPs or FITC-ZMO-E5-NPs solution was added to the dish and co-cultured for 2 h. Subsequently, the cells were washed three times with PBS and photographed using a Leica TCS SP8 STED confocal microscope. The fluorescence intensity of the cellular uptake images was quantified using Image J software (National Institutes of Health, Image J 2.1, USA).

2.16. In vitro hemocompatibility test

Mice ocular blood was withdrawn and mixed with an equal volume of physiological saline, gently mixed, and centrifuged at 3000 rpm for 5 min. The supernatant was discarded, and the washing continued until the supernatant was colorless. Then, 1 ml blood was diluted with 1.25 ml physiological saline.

100 μl diluted whole blood sample was added to solutions of different concentrations of free Nin, E5-NPs-Nin, ZMO-E5-NPs-Nin, ASO, E5-NPs-ASO and ZMO-E5-NPs-ASO (50 to 800 ng/ml). The samples were then incubated at 37 °C for 1 h. Subsequently, the solutions were centrifuged at 3000 rpm for 5 min. The absorbance of the supernatant was measured at 540 nm using a microplate reader (Bio-Tek, μQuant, USA). Distilled water and physiological saline were used as positive and negative controls, respectively.

2.17. *In vivo animal studies*

In vivo study established a 14-d BLM-induced mouse IPF model. Sixty male C57BL/6 J mice (6–8 weeks old, weighing 20–22 g) were purchased from Weitong Lihua Experimental Animal Technology Co., Ltd. and housed at the Nankai University Laboratory Animal Center (ambient conditions: 22–26 °C, humidity 60% ± 2%, 12 h light/dark cycle, *ad libitum* access to food and water). The animal experiments were approved by the Institutional Animal Care and Use Committee of Nankai University (approval number: SYDWLL-000098) and strictly followed relevant guidelines.

During modeling, except for the CTL group, which received an equal volume of physiological saline via intratracheal instillation, all other mice were administered 2 U/kg BLM, after which the tracheal incision was sutured. About 7 d after modeling, the mice were randomly divided into two major treatment experimental groups for intervention, with each subgroup containing eight animals. Experiment 1 (targeting nintedanib treatment) groups were: CTL, BLM, Nin (oral gavage, 60 mg/kg/d), Nin (intravenous, 6 mg/kg/every other day), E5-NPs, E5-NPs-Nin, ZMO-E5-NPs-Nin (intravenous, 6 mg/kg/every other day). Experiment 2 (targeting ASO treatment) groups were: CTL, BLM, ASO (intravenous, 2.5 mg/kg), ZMO-E5-NPs-Nin (intravenous, 6 mg/kg/every other day), ZMO-E5-NPs-ASO (intravenous, 2.5 mg/kg). All treatment groups were administered via tail vein injection every other day (except for the oral gavage group), while the BLM group received an equal volume of physiological saline as a positive control during the same period. 14 d after modeling, all mice underwent CT scanning, pulmonary function testing, and sample collection.

2.18. *Hydroxyproline content detection*

The right lung of the mouse was separated and placed in a 5 ml brown glass bottle, dried, and hydrolyzed under high temperature with acid. The pH was adjusted to 6.5–8.0, filtered, and adjusted to a total volume of 10 ml with PBS. To each tube, 350 μl H_2O and 50 μl sample were added, followed by 200 μl Chloramine-T. After vortexing the samples, they were left to stand at room temperature for 20 min, then 200 μl perchloric acid was added to each tube, vortexed, and left to stand at room temperature for 5 min. Then, 200 μl P-DMAB was added, vortexed, and incubated in a 50 °C water bath for 20 min. After cooling, 200 μl of each sample was taken to a 96-well plate, and the absorbance was measured at 577 nm.

2.19. *BALF cell count*

Bronchoalveolar lavage fluid (BALF) was collected for the analysis of inflammatory cytokines and total cell count. BALF was centrifuged at 4 °C and 1400 g for 10 min, the pellet was taken, resuspended in sterile PBS, and the total number of cells was counted using a hemocytometer.

2.20. *Histological analysis*

The left lungs from C57BL/6 J mice of different groups were fixed in 4% paraformaldehyde for 48 h. They were routinely embedded in paraffin and cut into 5-micrometer thick sections using a sledge microtome. Paraffin sections were stained with HE staining kit, Masson's trichrome staining kit, Sirius Red staining kit (Solarbio Science & Technology Co., Ltd, Beijing, China). Images were analyzed and quantified using Image J software (National Institutes of Health, Image J 2.1, USA).

2.21. *Immunofluorescence staining*

Cells or tissue sections were fixed with 4% paraformaldehyde for 30 min and permeated with 1% Triton X-100 for 10 min. After blocking with 3% bovine serum albumin for 1 h, cells were incubated with rabbit anti-α-SMA, rabbit anti- COL1A1, rabbit anti-CTGF at 37 °C for 2 h. After washing with PBS containing 1% Tween-20, the sections were incubated with the secondary antibody conjugated with Alexa Fluor 488 (Abcam, Cambridge, UK). Tissues were counterstained with DAPI. All images were captured using a Leica TCS SP8 STED confocal microscope.

2.22. *Statistical analysis*

Statistical analysis was performed using GraphPad Prism 9.0 software as the mean ± SD (GraphPad software, Inc., USA). All statistical comparisons were analyzed using one-way ANOVA, and the Tukey-Kramer test was used to determine significant differences between groups. $P < 0.05$ was considered statistically significant.

3. Results and discussion

3.1. *Preparation and characteristics of ZMO*

Firstly, we extracted MO from mouse bone marrow and then prepared ZMO, as shown in Fig. 2A. Scanning electron microscopy (SEM) images revealed that, compared with MO, ZMO maintained a normal cellular morphology, but with increased surface roughness. The average size of ZMO shows no significant difference compared to MO (Fig. 2B). Observations under an optical microscope showed that, compared with MO, ZMO could maintain a normal cellular morphology in PBS for a longer period (Fig. 2C). Confocal laser scanning microscopy results indicated that propidium iodide (PI) entered the majority of ZMO cells, while the PI fluorescence intensity in MO was negligible, proving that MO

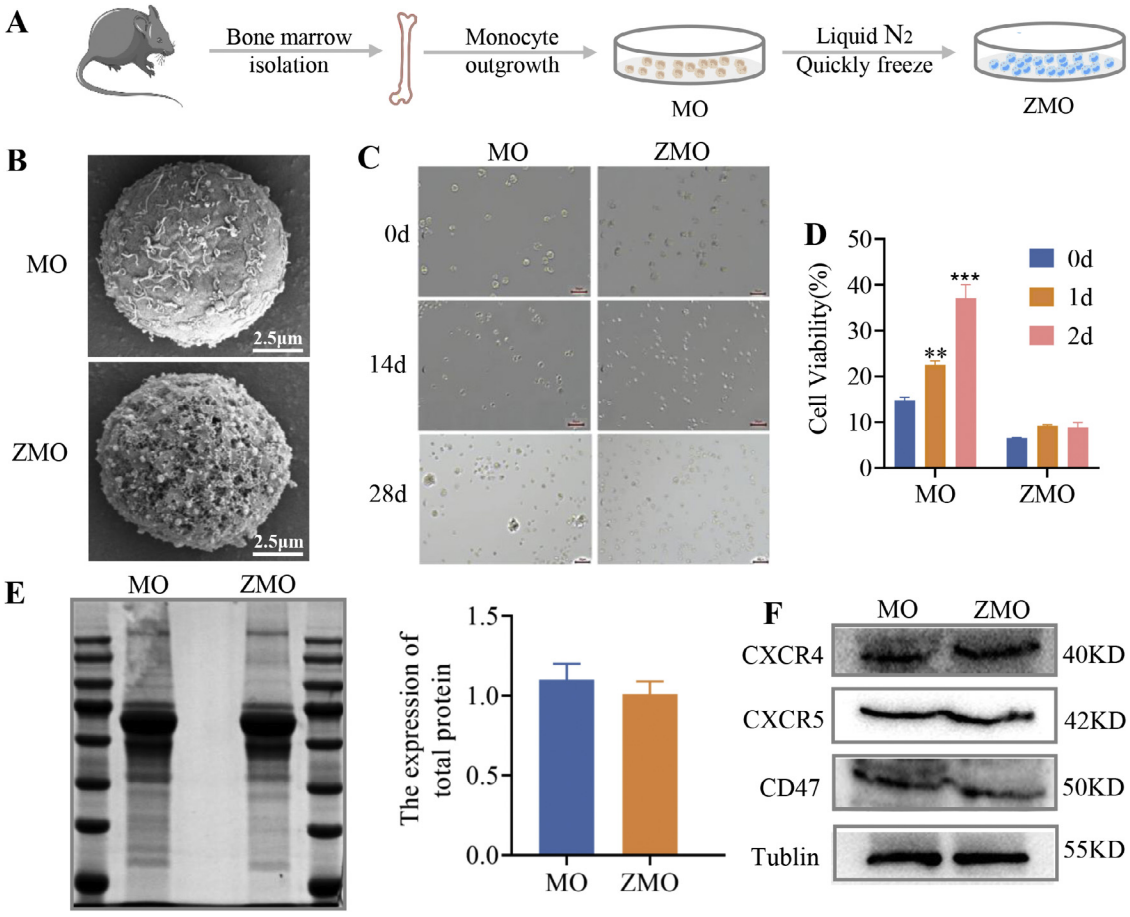


Fig. 2 – Preparation and characterization of cryo-shocked bone marrow mononuclear cells. (A) Schematic illustration of the preparation of cryo-shocked bone marrow mononuclear cells; (B) SEM images of MO and ZMO, scale bar: 5 μm; (C) Cellular morphology of MO and ZMO suspended in PBS observed at 0, 14 and 28 d, scale bar: 50 μm; (D) Cell proliferation of MO and ZMO at 0, 1 and 2 d; (E) Total protein content on the cell membrane of MO and ZMO observed by Coomassie Brilliant Blue and data analysis; (F) Western blotting results of characteristic surface proteins CXCR4, CXCR5 and CD47 on the cell membrane of MO and ZMO. All statistical analyses were performed using one-way ANOVA ($n \geq 3$, The cell count of MO on Day 0 as a control, *P ≤ 0.05, **P ≤ 0.01, ***P ≤ 0.001).

was indeed killed by liquid nitrogen freezing to become ZMO (Fig. S1B). Flow cytometry forward scatter and side scatter information also demonstrated that the internal complexity of MO and ZMO was similar (Fig. S1A). In terms of cell proliferation, unlike the stable proliferation results of MO, ZMO showed that it lacked the ability to proliferate (Fig. 2D). To explore whether ZMO still has the ability to couple peptide molecules on its membrane surface and resist phagocytosis, we extracted the cell membrane surface proteins of MO and ZMO. Coomassie Brilliant Blue and Western Blot results showed that, compared with MO, there was no significant difference in the total protein amount and the expression of characteristic proteins such as CXCR4 and CD47 on the cell membrane surface of ZMO (Fig. 2E and 2F). All the above results prove that after liquid nitrogen freezing, ZMO no longer has the ability to perform biological behaviors, but its overall morphology, size, and cell membrane surface characteristic proteins are not significantly different from MO.

CD47, a widely expressed transmembrane glycoprotein, transmits a "don't eat me" signal by binding to signal regulatory protein α on immune cells, thereby inhibiting phagocytosis [22]. CXCR4 is an important chemokine receptor. The preservation of these key membrane proteins holds significant implications: the presence of CD47 may enable ZMO to partially evade clearance by the mononuclear phagocyte system [23], while the retention of CXCR4 provides the foundation for subsequent specific binding with targeting peptides [24]. Together, these results demonstrate that although ZMO loses its biological activity, it completely retains its cellular morphology, size and critical membrane surface proteins, laying the groundwork for constructing a cell-based delivery system.

3.2. *Characterization of ZMO-E5-NPs*

Subsequently, we synthesized MO-E5-NPs and ZMO-E5-NPs. The purity identification results of peptide E5 are shown in Fig. S2A and S2B. It was then connected with DSPE-PEG-MAL to obtain DSPE-PEG-MAL-E5 (Fig. 3A). 1H NMR spectroscopy showed that the characteristic peaks of E5 were between 3.55–3.63, 3.54–3.55 and 2.51–2.52, which are in the same range as the literature, confirming that peptide

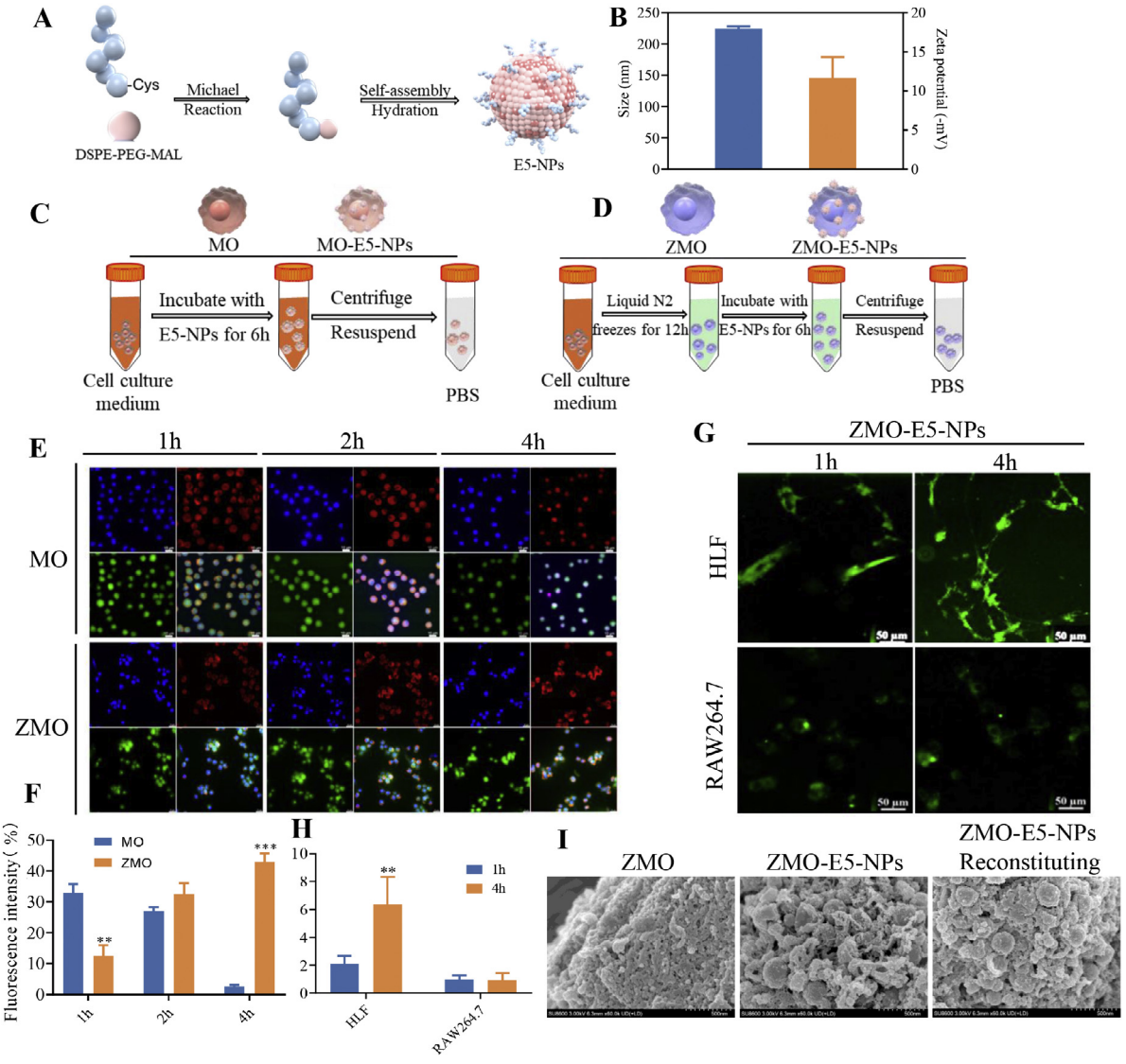


Fig. 3 – Preparation and characterization of ZMO-E5-NPs. (A) Schematic illustration of the synthesis of DSPE-PEG-MAL-E5 and the construction of E5-NPs; (B) Particle size and zeta potential graph of E5-NPs; (C) Schematic of the conjugation process between MO and E5-NPs; (D) Schematic of the conjugation process between ZMO and E5-NPs; (E) Carrier stability results after MO and ZMO were connected with FITC-E5-NPs for 1, 2 and 4 h. Blue represents Hoechst 33342, indicating the cell nucleus; red represents Dil membrane dye staining the membranes of MO and ZMO cells; green represents FITC, indicating E5-NPs. Scale bar: 10 μm; (F) Uptake of ZMO-FITC-E5-NPs by HLF cells and RAW264.7 cells. Scale bar: 50 μm; (G) Analysis of cellular uptake fluorescence intensity. (H) Statistical analysis of the fluorescence intensity of HLF and RAW264.7 cells after 2h and 4h of uptake of ZMO-E5-NPs; (I) Scanning electron microscopy images of ZMO, ZMO-E5-NPs, and freeze-dried and reconstituted ZMO-E5-NPs, scale bar: 500nm. All statistical analyses were performed using one-way ANOVA (The fluorescence intensity of E5-NPs as a control, *P ≤ 0.05).

E5 has been successfully connected with DSPE-PEG-MAL (Fig. S2C). Infrared spectroscopy also proved this (Fig. S3A). Malvern particle size analyzer measured the particle size distribution index (PDI) and Zeta potential of E5-NPs to be 224.7 ± 3.260 nm and −11.68 ± 2.674 mV, respectively (Fig. 3B). The synthesis process of MO-E5-NPs is shown in Fig. 3C, and the synthesis process of ZMO-E5-NPs is shown in Fig. 3D In the immunofluorescence experiment, E5 labeled with FITC exhibits green fluorescence, and Dil staining of the cell membrane shows red fluorescence. During the 1 h incubation process, there is a clear orange fluorescence colocalization on the cell membrane surface, indicating that both ZMO-E5-NPs and MO-E5-NPs are relatively stable. However, after 4 h, compared to ZMO-E5-NPs, the orange fluorescence of MO-E5-NPs is diminished, and the connection with E5-NPs is unstable (Fig. 3E and F). The conjugation efficiency between E5-NPs and ZMO is approximately 20%. To evaluate the anti-phagocytosis and cellular uptake of ZMO-E5-NPs, we selected LPS-induced macrophages and primary lung fibroblasts from IPF patients as models to evaluate

the uptake performance and immune escape function of ZMO-E5-NPs. Confocal results and data analysis indicated that in LPS-stimulated HLF, the uptake of E5-NPs by cells increased over time, while there was no significant change in fluorescence intensity in LPS-induced RAW264.7 cells (Fig. 3G and 3H). This proves that ZMO-E5-NPs have a certain degree of immune evasion, can reduce the clearance of NPs by the MPS system, but can improve the uptake of drugs by lung fibroblast cells in an inflammatory environment. This result suggests that ZMO-E5-NPs may achieve a certain degree of immune evasion through the surface-retained CD47-mediated "don't eat me" signal, thereby reducing clearance by the phagocytic system [22,24]. Additionally, we further assessed the binding efficiency of the peptide E5 to CXCR4 using flow cytometry. The results revealed that the E5 binding efficiency was significantly reduced in the CXCR4 inhibitor (AMD3100)-treated group compared to the ZMO + E5-NPs group (Fig. S3C). These findings demonstrate that CXCR4 plays a critical role in the targeted interaction between ZMO and E5-NPs, and that blocking its function effectively disrupts this specific binding. These findings are consistent with previous studies, indicating that CXCR4 serves as a crucial receptor mediating targeted interactions [23]. SEM results indicated that the surface of ZMO appeared smooth without nanoparticle binding, whereas abundant nanoparticle attachment was observed on the surface of ZMO-E5-NPs. Furthermore, the lyophilized and reconstituted ZMO-E5-NPs maintained stable morphological characteristics (Fig. 3I).

3.3. *ZMO-E5-NPs exhibit inflammatory targeting*

To further verify whether the E5-NPs carrier can "hitchhike" through the inflammatory homing effect of ZMO to deliver to the lesion site and increase the drug concentration at the inflammatory site, we designed a mouse foot swelling inflammation model and a BLM-induced early IPF model for experiments. The results showed that the ZMO-E5-Cy7.5-NPs group had the highest foot fluorescence intensity, followed by the E5-Cy7.5-NPs group, and the weakest in the Cy7.5 group (Fig. 4A and 4B). The experiment confirmed that ZMO-E5-NPs can effectively accumulate at the inflammatory site. This result aligns with the study by Xu et al. using "zombie" macrophages for targeted drug delivery [14], sharing a similar concept, and confirms that engineered immune cell-based carriers exhibit favorable inflammatory chemotaxis. The BLM model is widely utilized due to its simple operation, high reproducibility, and ability to simulate key features of human IPF [25]. To better simulate the accumulation of ZMO-E5-NPs in the pulmonary fibrosis lung tissue, we constructed a BLM-induced IPF model, which mainly shows inflammatory infiltration before 7 d and develops into a coexistence of inflammation and fibrosis process after 7 d. The *ex vivo* results showed that the ZMO-E5-Cy7.5-NPs group had the strongest fluorescence in lung tissue, of course, there was also a certain degree of enrichment in liver and kidney tissues (Fig. 4C and 4D). In summary, the above experiments have demonstrated that ZMO-E5-NPs possess a certain inflammatory homing effect and can effectively target inflamed lung tissue. We further simulated the *in vitro* release of E5-NPs-Nin and ZMO-E5-NPs-Nin. In the co-culture medium of LPS-induced macrophages and HLFs, the cumulative release rates of E5-NPs and ZMO-E5-NPs were 27.21% ± 5.76% and 31.44% ± 6.619%, respectively (Fig. 4E). In the recombinant MMP2 protein solution, the cumulative release rates of E5-NPs and ZMO-E5-NPs were also 74.61 ± 1.166 and 76.83 ± 1.166, respectively (Fig. 4F). The results indicate that ZMO-E5-NPs can accelerate drug release and enhance drug utilization in conditions of high inflammation and high MMP2 expression.

3.4. *ZMO-E5-NPs-Nin effectively inhibits BLM-Induced pulmonary fibrosis in mice*

Nintedanib is a multi-target tyrosine kinase inhibitor that targets receptors such as PDGF, FGF and VEGF, possessing anti-fibrotic and anti-inflammatory effects. It is currently an important approved drug for the treatment of progressive chronic fibrosing interstitial lung disease [26,27]. In order to better verify whether ZMO-E5-NPs can successfully deliver drugs to lung tissue and alleviate the progression of pulmonary fibrosis, we first prepared a drug delivery system with ZMO-E5-NPs encapsulating nintedanib (ZMO-E5-NPs-Nin). EE of nintedanib was determined to be 96% ± 9.12%, and drug loading capacity (LC) was found to be 16.35% ± 1.195%. PDI and Zeta potential of E5-Nin were 236.1 ± 4.438 nm and −14.53 ± 0.1528 mV, respectively (Fig. S4A).

Additionally, we assessed the toxicity of ZMO-E5-NPs-Nin to HLF cells. At relatively low concentrations of Nin (≤200 ng/ml), ZMO-E5-NPs-Nin showed no significant cytotoxicity (Fig. S4B). In the development and research of nanomedicines, it has been found that nanomedicines may cause adverse reactions, and some biomaterials even have potential high hemolytic risks. We evaluated the hemolytic risk of Nin, E5-NPs-Nin and ZMO-E5-NPs-Nin. The results showed that at drug concentrations of 50–800 ng/mL, the hemolysis rates of Nin, E5-NPs-Nin and ZMO-E5-NPs-Nin were all below 5% compared to the positive control group (Fig. S4C and S4D), indicating that the NPs meet the hemolytic requirements for biomaterials. Under pathological conditions of IPF, α-SMA is significantly overexpressed and is an important marker in the development of IPF. Therefore, we also compared the effects of Nin, E5-NPs-Nin and ZMO-E5-NPs-Nin on the expression of α-SMA in pathological states of NIH 3T3 cells. The results showed that after delivery of Nin via ZMO-E5-NPs, the expression of α-SMA was significantly reduced (Fig. S4E and S4F).

We finally assessed the *in vivo* efficacy of ZMO-E5-NPs-Nin in inhibiting pulmonary fibrosis in mice. The animal experimental model is shown in Fig. 5A. The hydroxyproline content in the lung tissue of each group of mice was measured, and the ZMO-E5-NPs-Nin group had the lowest hydroxyproline content (Fig. 5B). BALF was collected to determine the number of inflammatory cells, and the results showed that the ZMO-E5-NPs-Nin group had the least inflammatory cell infiltration in the lung tissue (Fig. 5C). Before sacrificing the mice, lung function was measured for each group, and the results showed that the ZMO-E5-NPs-Nin group had the best recovery of lung function (Fig. 5D-G). The reconstructed CT images showed that the BLM group had severe pulmonary fibrosis and loss of lung parenchyma, while the fibrosis was significantly improved after treatment, especially in the ZMO-E5-NPs-Nin group

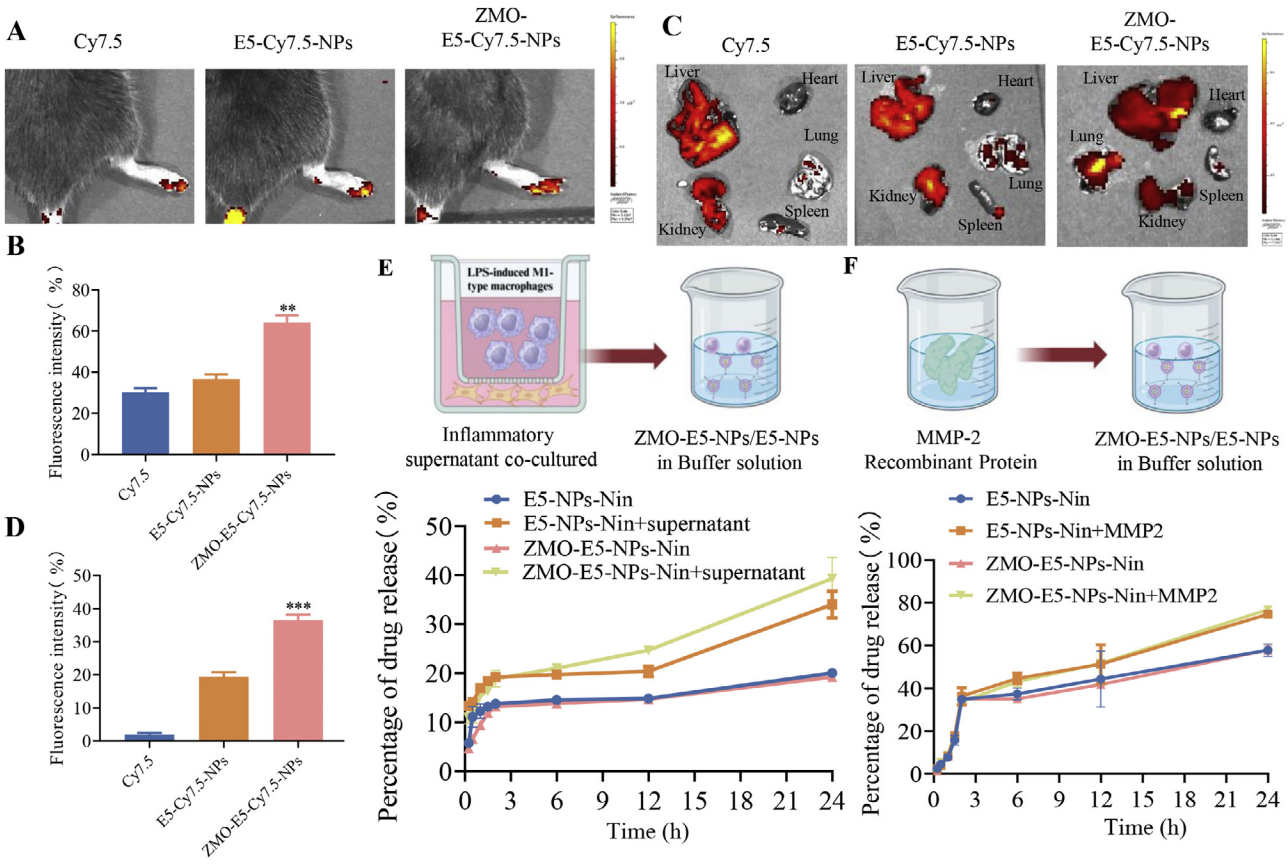


Fig. 4 – *In vivo* validation of the inflammatory homing targeting of ZMO-E5-NPs. (A) A mouse right hind paw edema model was constructed, and Cy7.5, Cy7.5-E5-NPs, ZMO–Cy7.5-E5-NPs were tail vein injected, followed by IVIS imaging after 1 h. Quantitative analysis was also performed ($n \geq 3$); (B) The same as above, but with quantitative analysis; (C) *Ex vivo* imaging to observe the biodistribution of Cy7.5, Cy7.5-E5-NPs, ZMO–Cy7.5-E5-NPs in various organs of IPF mice ($n \geq 3$); (D) The same as above, but with quantitative analysis; (E) Cumulative release rates and schematic diagram of E5-NPs and ZMO-E5-NPs in the co-culture supernatant of LPS-induced macrophages and HLFs; (F) Cumulative release rates and schematic diagram of E5-NPs and ZMO-E5-NPs in the recombinant human MMP2 protein solution. All statistical analyses were performed using one-way ANOVA ($n \geq 3$, fluorescence intensity of E5-NPs as a control, *P ≤ 0.05, **P ≤ 0.01, ***P ≤ 0.001).

(Fig. 5H). Subsequently, through data processing, the cross-section, coronal, and sagittal views (Fig. S5A) as well as 3D images of the lungs were constructed according to the fully aerated volume (red), non-aerated volume (yellow), and partially aerated volume (blue). Data analysis of the images and group lung volume showed that the ZMO-E5-NPs-Nin group had the least non-aerated lung volume compared to the BLM group (Fig. 5I-5K). We then evaluated the fibrosis and collagen deposition in the mice's lungs through H&E, Masson's trichrome, and Sirius Red staining. The BLM group showed severe loss of lung parenchyma, increased alveolar diameter, and thickened alveolar walls compared to the normal group. Inflammatory cell infiltration, including macrophages, was also observed in the lung tissue. Compared with the BLM group, E5-NPs did not have any therapeutic effect because they did not carry any drugs. However, the necrotic areas were reduced in the Nin (i.g.), Nin (i.v.), E5-Nin, and ZMO-E5-Nin groups, with the targeted ZMO-E5-Nin group showing the most significant therapeutic effect. In addition, Masson's trichrome and Sirius Red staining showed that the ZMO-E5-Nin group had less inflammatory cell infiltration and more normal bronchiolar structures compared to other treatment groups. Moreover, compared with the BLM group, the collagen deposition in the blue areas after treatment with the ZMO-E5-Nin group was significantly reduced (Fig. 5L). Statistical analysis of the fibrotic area also proved this conclusion (Fig. S5B-S5D). Additionally, as shown in Fig. S5E, HE staining and Masson staining results revealed that the ZMOs-only group did not exhibit significant anti-fibrotic effects, indicating that the therapeutic contribution of the cellular component itself is limited. The physical mixture group (ZMOs + E5-NPs) showed some therapeutic efficacy, but it remained significantly lower than that of the carrier group (ZMO-E5-NPs). In addition, RT-PCR results showed that the expression of α-SMA, Col-1, Fn, IL-1β and IL-6 factors in the ZMO-E5-Nin group was significantly reduced compared with the BLM group (Fig. 5M and S6A&S6B). Immunofluorescence staining also proved that ZMO-E5-Nin significantly reduced the deposition of α-SMA and Col-1 in the lungs of mice (Fig. S6C). This is consistent with the growing trend of using nintedanib as a positive control

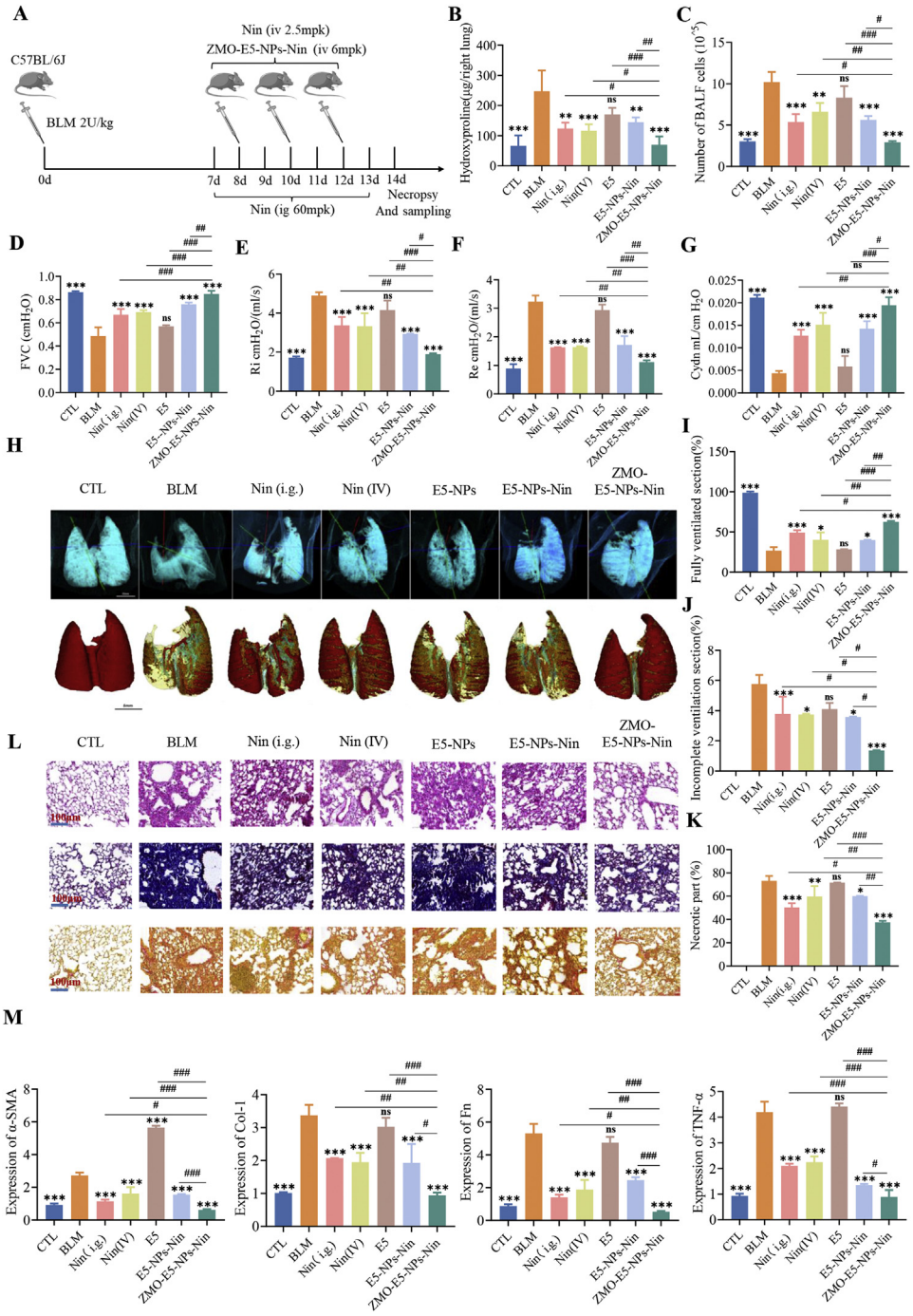


Fig. 5 – *In vivo* anti-fibrotic efficacy of ZMO-E5-NPs-Nin. (A) Schematic diagram of IPF modeling and treatment; (B) Hydroxyproline expression in mouse lung tissue; (C) Number of inflammatory cells in mouse bronchoalveolar lavage fluid; (D-G) Mouse lung function (FVC, Ri, Re, Cdyn); (H) Lung CT images and 3D images of mice on Day 13 of modeling (scale bar: 10 mm), with red representing fully aerated areas, yellow representing non-aerated areas, and blue representing partially aerated areas; (I-K) Data analysis of the fully ventilated section, incomplete ventilation, and necrotic part; (L) Histological evaluation of lung tissue sections from mice after different treatments using H&E staining, Masson's trichrome staining, and Sirius Red staining to assess lung lesions and collagen deposition (scale bar: 100 μm); (M) Comparative analysis of the expression of fibrotic factors in mouse lung tissue (α-SMA, Col-1, Fn, TNF-α). All statistical analyses were performed using one-way ANOVA ($n \geq 3$, group of BLM as a control, *P ≤ 0.05, **P ≤ 0.01, ***P ≤ 0.001).

in BLM models [28] and highlights the advantages of targeted delivery.

3.5. *In vitro anti-fibrotic effect validation of ASO and characterization of ZMO-E5-NPs-ASO properties*

ASOs regulate gene expression by targeting pre-mRNA or mRNA sequences, offering a unique strategy for disease intervention at the root cause [20]. Compared to traditional drugs that target proteins, ASOs possess higher druggability potential, particularly for refractory diseases [21]. Subsequently, we designed ASO sequences targeting CTGF, with the specific sequence information shown in Fig. 6A. To enhance stability and cellular uptake, we modified the ASOs with locked nucleic acid (LNA) and phosphorothioate (PS) modifications [29,30]. We first verified the silencing effect of ASO in NIH-3T3 cells and its cytotoxicity. PCR and WB results showed that LNA-CTGF ASO dose-dependently inhibited CTGF expression (Fig. 6B and S7A&S7B), and it did not show significant cytotoxicity in the range of 10–200 nM (Fig. 6C). Then, we used TGF-β1 to induce NIH-3T3 to mimic the cellular state under IPF pathological conditions. After transfection of LNA-CTGF ASO into cells for 24 h, the expression of fibrotic factors such as CTGF, α-SMA and Col-1 was also dose-dependently inhibited (Fig. 6D-6F). Nintedanib is a multi-tyrosine kinase inhibitor that mainly delays the progression of IPF by inhibiting the activation of fibroblasts and collagen secretion. By setting a gradient of nintedanib in NIH-3T3 cells, 5 μM was confirmed as a non-toxic and effective dose to serve as a positive control for ASO (Fig. 6G). To verify whether ASO has an inhibitory effect on the migration of NIH 3T3 induced by TGF-β1, we set up a cell scratch assay. The results showed that compared with the cells treated with TGF-β1, the cells treated with Nin and ASO had slower scratch healing, proving that ASO can effectively inhibit the migration of cells stimulated by TGF-β1 (Fig. 6H). In addition, confocal results also proved that ASO can reduce the expression of CTGF (Fig. 6I and S7C) and α-SMA (Fig. S7C and S7D).

The above experimental results confirmed that the ASO we constructed can effectively inhibit the activation of lung fibroblasts and EMT. To further verify its *in vivo* efficacy, we encapsulated ASO with a carrier to obtain the ZMO-E5-NPs-ASO drug delivery system. Then, we used the thin-film hydration method to encapsulate LNA-CTGF ASO in E5-NPs to determine its EE. The EE of E5-NPs-ASO was measured to be 55 ± 8.47%, while its LC was determined as 9.750% ± 1.237%. PDI and Zeta potential of E5-ASO were 232.1 ± 2.10 nm and −8.887 ± 2.399 mV, respectively (Fig. 6J).

To verify whether ZMO-E5-NPs encapsulating ASO would be toxic to cells *in vivo*, we assessed the safety of ZMO-E5-NPs-ASO on 3T3 cells. At relatively low concentrations of ASO (≤200 ng/ml), ZMO-E5-ASO showed no significant cytotoxicity to cells (Fig. 6K). We also evaluated the hemolytic risk, where the results showed that at drug concentrations of 50–800 ng/ml, the hemolysis rates of ASO, E5-NPs-ASO and ZMO-E5-NPs-ASO were all below 5% compared to the positive control group (Fig. 6L and S7E), indicating that the NPs met the hemolytic requirements for biomaterials. At the same time, we also compared the effects of ASO, E5-NPs-ASO, and ZMO-E5-NPs-ASO on the expression of α-SMA in pathological states of NIH 3T3. The results showed that after delivery of ASO via ZMO-E5-NPs, the expression of α-SMA was significantly reduced (Fig. S7F and S7G).

3.6. *ZMO-E5-NPs-ASO inhibits BLM-Induced pulmonary fibrosis in mice*

The animal experimental model is depicted in Fig. 7A. The hydroxyproline (an amino acid characteristic of collagen, whose levels reflect the degree of fibrosis [31]) content in the lung tissue of the mice was measured, revealing that the ZMO-E5-NPs-ASO group had the lowest hydroxyproline content (Fig. 7B). BALF was collected to determine the number of inflammatory cells, and it was found that the ZMO-E5-NPs-Nin group had the least inflammatory cell infiltration in the lung tissue (Fig. 7C). Prior to the sacrifice of the mice, lung function was measured for each group. Compared to the ASO group and the ZMO-E5-NPs-Nin group, the ZMO-E5-NPs-ASO group showed the best recovery of lung function (Fig. 7D-7G). On Day 13 after modeling, CT scans of the mice's lungs were taken to observe the progression of IPF. The reconstructed CT images showed severe pulmonary fibrosis and loss of lung parenchyma in the BLM group, which was significantly improved after treatment, especially in the ZMO-E5-NPs-ASO group (Fig. 7H). Subsequent data processing constructed cross-sectional, coronal, and sagittal views (Fig. S8A) as well as 3D images of the lungs, divided into fully aerated volume (red), non-aerated volume (yellow), and partially aerated volume (blue). Data analysis of the images and group lung volume indicated that the ZMO-E5-NPs-ASO group had the least non-aerated lung volume compared to the BLM group (Fig. 7I-7K).

We then assessed the fibrosis and collagen deposition in the mice's lungs through H&E, Masson's trichrome and Sirius Red staining. The BLM group showed severe loss of lung parenchyma, increased alveolar diameter, and thickened alveolar walls compared to the normal group. Inflammatory cell infiltration, including macrophages, was also observed in the lung tissue. In contrast to the BLM group, E5-NPs, which did not carry any drugs, did not have any therapeutic effect. However, the necrotic areas were reduced in the ASO and ZMO-E5-NPs-Nin groups, with the targeted ZMO-E5-NPs-ASO group showing the most significant therapeutic effect due to its targeting capabilities. Moreover, Masson's trichrome and Sirius Red staining showed that the ZMO-E5-NPs-ASO group had reduced inflammatory cell infiltration and more normalized bronchiolar structures compared to other treatment groups. Additionally, compared to the BLM group, the collagen deposition in the blue areas after treatment with the ZMO-E5-NPs-ASO group was significantly reduced (Fig. 7L). Statistical analysis of the fibrotic area also confirmed this conclusion (Fig. S8B-S8D). Furthermore, we compared the expression of lung fibrosis (Fig. 7M) and inflammatory factors in each group of mice (Fig. S9A-S9B). RT-PCR results showed that the expression of CTGF, α-SMA, Col-1, Fn, IL-1β and IL-6 factors in the ZMO-E5-NPs-ASO group was significantly reduced compared to the BLM group (Fig. 7M). Immunofluorescence staining also demonstrated that ZMO-E5-NPs-ASO significantly reduced the deposition of α-SMA and Col-1 in the lungs of mice (Fig. S9C-S9E). Furthermore, we examined the Smad signaling pathway, which is closely

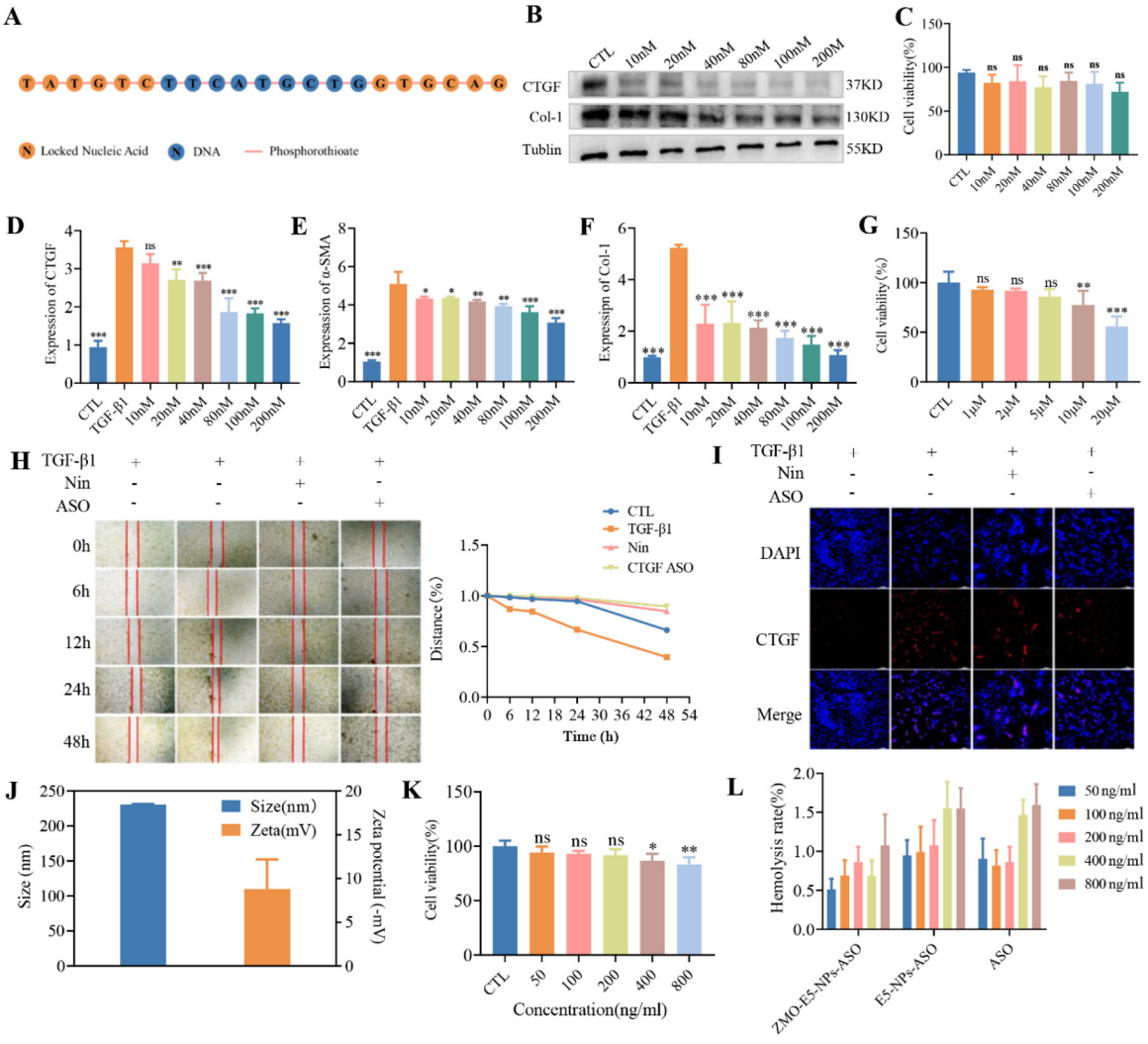


Fig. 6 – Design and *in vitro* anti-fibrotic efficacy verification of LNA-CTGF ASO. (A) Schematic diagram of LNA-CTGF ASO sequence and modification method; (B) Gradient inhibition of CTGF and Col-1 expression in NIH-3T3 cells treated with LNA-CTGF ASO at concentrations of 10–200 nM; (C) The effect of LNA-CTGF ASO at concentrations of 10–200 nM on the viability of NIH-3T3 cells; (D-F) Gradient inhibition of protein expression of CTGF, α-SMA and Col-1 in NIH-3T3 cells stimulated with TGF-β1 and treated with LNA-CTGF ASO at concentrations of 10–200 nM; (G) Effect of nintedanib at concentrations of 1–20 μM on the viability of NIH-3T3 cells, using 5 μM Nin as a positive control for ASO; (H) Effect of different treatments on the migration of NIH-3T3 cells, with statistical analysis of cell migration rates after 0–48 h of treatment (scale bar: 200 μm); (I) Immunofluorescence staining of CTGF in NIH-3T3 cells after different treatments (scale bar: 100 μm); (J) Particle size and zeta potential graph of E5-NPs-ASO; (K) Effect of ASO content in ZMO-E5-NPs-ASO at concentrations of 50–800 ng/ml on the viability of NIH-3T3 cells; (L) Biocompatibility of ASO, E5-NPs-ASO, ZMO-E5-NPs-ASO at concentrations of 50–800 ng/ml, with H_2O as a positive control and 0.9% physiological saline as a negative control. Measurement of supernatant hemolysis rate not exceeding 5%. All statistical analyses were performed using one-way ANOVA ($n \geq 3$, *P ≤ 0.05, **P ≤ 0.01, ***P ≤ 0.001).

associated with fibrosis. The results revealed that ZMO-E5-NPs-ASO significantly inhibited the phosphorylation of Smad2 and Smad3 in mouse lung tissues (Fig. S9F-S9G). These findings demonstrate that ZMO-E5-NPs-ASO alleviates the progression of IPF by suppressing CTGF expression and thereby regulating the activation of Smad2/3 signaling. It is worth noting that the anti-fibrotic effect of ZMO-E5-NP-ASO is significantly better than that of the ZMO-E5-NP-Nin and ASO groups.

To further comprehensively validate the biosafety of the carrier system, we performed additional histopathological examinations of key organs including the liver and kidney using H&E staining. As demonstrated in Fig. S10A, no significant pathological changes were observed in any treatment groups (ZMO-E5-NPs, ZMO-E5-NPs-Nin and ZMO-E5-NPs-ASO) compared to the control group, providing direct morphological evidence for the safety of the materials at the tissue level. Moreover, to preliminarily evaluate systemic

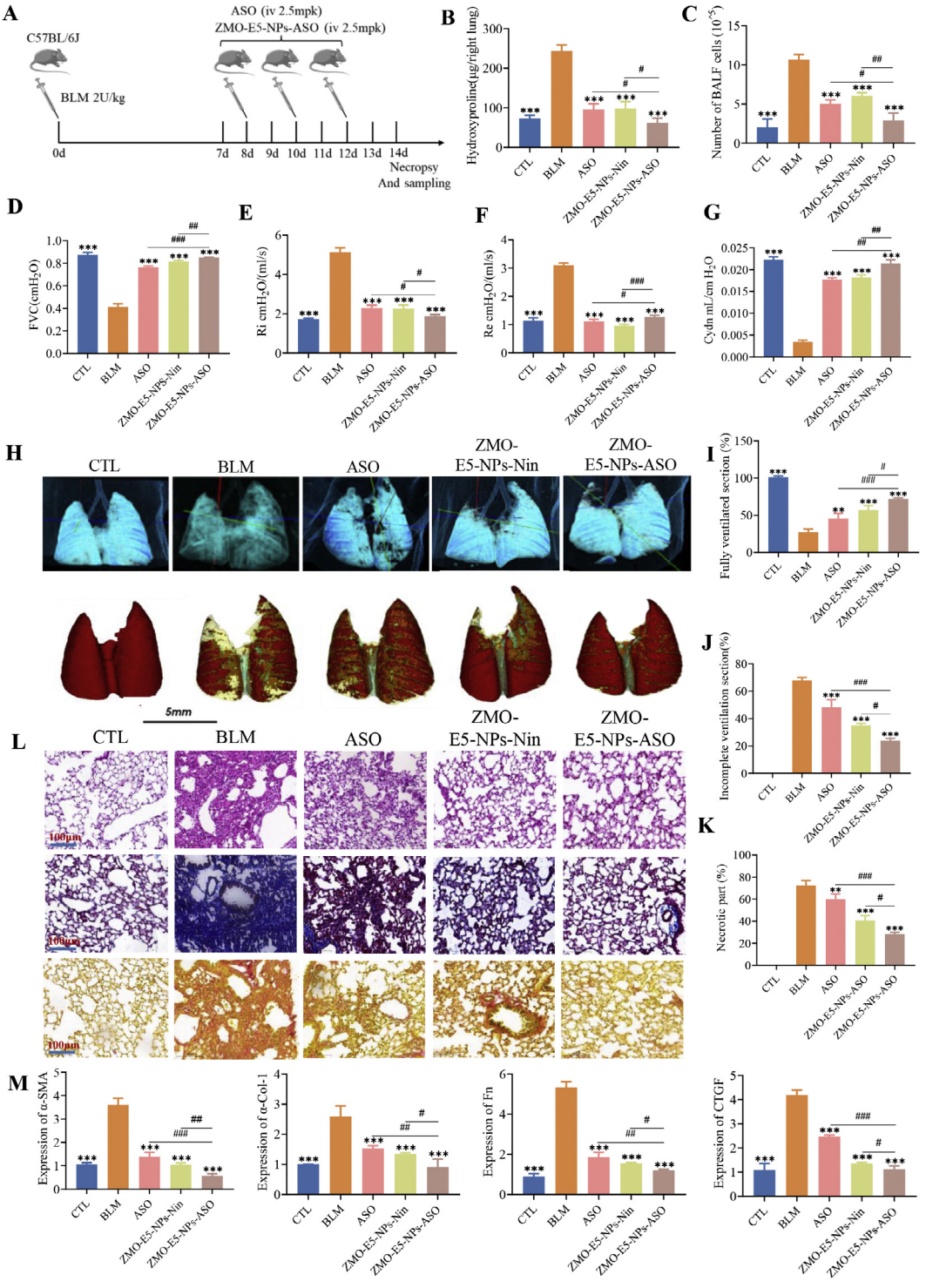


Fig. 7 – *In vivo* anti-fibrotic efficacy of ZMO-E5-NPs-ASO. (A) Schematic diagram of IPF modeling and treatment; (B) Comparative analysis of hydroxyproline expression in mouse lung tissue; (C) Comparative analysis of the number of inflammatory cells in mouse bronchoalveolar lavage fluid; (D-G) Comparative analysis of mouse lung function (FVC, Ri, Re, Cdyn). (H) Lung CT images on Day 13 of modeling (Scale bar: 10 mm) and 3D images (Scale bar: 5 mm), with red indicating fully aerated areas, yellow indicating non-aerated areas, and blue indicating partially aerated areas; (I-K) Data analysis of the fully ventilated section, incomplete ventilation, and necrotic part; (L) Histological evaluation of lung tissue sections from mice after different treatments using H&E staining, Masson's trichrome staining, and Sirius Red staining to assess lung lesions and collagen deposition (Scale bar: 100 μm); (M) Comparative analysis of the expression of fibrotic factors in mouse lung tissue (α-SMA, Col-1, Fn, CTGF). All statistical analyses were performed using one-way ANOVA ($n \geq 3$, The group of BLM as a control, *$P \leq 0.05$, **$P \leq 0.01$, ***$P \leq 0.001$).

inflammatory responses, we quantified the levels of key pro-inflammatory cytokines, TNF-α and IL-6, in serum via ELISA. The results revealed no statistically significant increase in these cytokines after administration (Fig. S10B), further supporting the absence of systemic inflammatory reactions. The serum ASO concentration peaked at 30 min after administration (Fig. S10C), and the exposure levels of naked ASO and ZMO-E5-NPs-ASO in the blood were similar. Notably, compared with naked ASO, the ASO content in the lung tissue of the ZMO-E5-NPs-ASO group was significantly higher at the same time points (Fig. S10D). These results collectively demonstrate that the ZMO-E5-NPs carrier can effectively deliver and enrich the drug in lung tissue.

4. Conclusion

In summary, this study developed a ZMO-E5-NPs drug delivery system and an ASO drug, and confirmed that ZMO-E5-NPs carrying ASO drugs can effectively inhibit the progression of IPF in mice, providing a new treatment strategy in the field of IPF treatment. The cryo-shocked monocyte-nanoparticle composite system (ZMO-E5-NPs) developed in this study shares the core concept of cell-mediated targeting with previous systems based on live immune cells (such as macrophage carriers) or cell membrane-coated systems (such as erythrocyte membrane nanoparticles). However, through the following innovative designs, we have addressed the bottlenecks of existing technologies. Compared to traditional delivery systems relying on the natural chemotaxis of cells, ZMO-E5-NPs extend the carrier storage time via cryo-shock technology, overcoming the clinical application limitations of live cells. Its MMP2-responsive E5 peptide design significantly enhances lesion accumulation efficiency and achieves a substantial increase in the intracellular internalization rate of ASO and nintedanib through a dual-cascade targeting mechanism of "monocyte homing - MMP2 activation - fibroblast capture."

However, the study still has many shortcomings. For instance, although ZMO-E5-NPs-ASO showed positive effects in the short term, the study did not involve the long-term effects and potential side effects, which require further research for assessment. Although ZMO-E5-NPs can target the lungs, their distribution and mechanism of action in different lung cell types still need further research to ensure that the drug can accurately act on the target cells. The study was conducted in animal models, and its effectiveness and safety in humans still need to be verified through clinical trials.

Conflicts of interest

The authors declare that there is no conflicts of interest.

CRediT authorship contribution statement

Hailong Li: Writing – review & editing, Writing – original draft, Funding acquisition. **Xi Wu:** Writing – review & editing, Writing – original draft, Formal analysis. **Jinhe Li:** Methodology. **Liqing Han:** Methodology, Formal analysis. **Hongting Liu:** Methodology. **Qiuyan Jiang:** Methodology. **Bowen Liu:** Methodology, Formal analysis. **Qin Xia:** Methodology. **Zherui Li:** Software. **Xiaohe Li:** Software, Resources, Formal analysis. **Songtao Gu:** Software, Formal analysis. **Aiguo Xu:** Software. **Honggang Zhou:** Supervision, Software, Methodology, Formal analysis. **Xiaoting Gu:** Writing – review & editing, Software, Formal analysis. **Zuojun Xu:** Supervision, Funding acquisition. **Xiaoyu Ai:** Supervision, Methodology, Formal analysis. **Cheng Yang:** Writing – review & editing, Writing – original draft, Supervision, Funding acquisition.

Acknowledgements

This work was supported by The National Natural Science Foundation of China (Grant Numbers 82400094, 82270069, 82370073), National High Level Hospital Clinical Research Funding (2022-PUMCH-B-108). We express our gratitude to the State Key Laboratory of Medicinal Chemical Biology, School of Pharmacy, Jinnan Campus, Nankai University, for providing laboratory facilities.

Supplementary materials

Supplementary material associated with this article can be found, in the online version, at doi:10.1016/j.ajps.2026.101128. The figures and tables with "S" before the serial number are included in the Supplementary material.

References

[1] Bonella F, Spagnolo P, Ryerson C. Current and future treatment landscape for idiopathic pulmonary fibrosis. Drugs 2023;83:1581–93.
[2] Podolanczuk AJ, Thomson CC, Remy-Jardin M, Richeldi L, Martinez FJ, Kolb M, et al. Idiopathic pulmonary fibrosis: state of the art for 2023. Eur Respir J 2023;61(4):2200957.
[3] Gan C, Wang Y, Xiang Z, Liu H, Tan Z, Xie Y, et al. Niclosamide-loaded nanoparticles (Ncl-NPs) reverse pulmonary fibrosis *in vivo* and *in vitro*. J Adv Res 2023;51:109–20.
[4] Kim JS, Murray S, Yow E, Anstrom KJ, Kim HJ, Flaherty KR, et al. Comparison of pirfenidone and nintedanib: post hoc analysis of the CleanUP-IPF study. Chest 2024;165:1163–73.
[5] John AE, Joseph C, Jenkins G, Tatler AL. COVID-19 and pulmonary fibrosis: a potential role for lung epithelial cells and fibroblasts. Immunol Rev 2021;302:228–40.
[6] Li Z, Niu S, Guo B, Gao T, Wang L, Wang Y, et al. Stem cell therapy for COVID-19, ARDS and pulmonary fibrosis. Cell Prolif 2020;53:e12939.
[7] Enomoto Y, Katsura H, Fujimura T, Ogata A, Baba S, Yamaoka A, et al. Autocrine TGF-β-positive feedback in profibrotic AT2-lineage cells plays a crucial role in non-inflammatory lung fibrogenesis. Nat Commun 2023;14:4956.
[8] Guan R, Yuan L, Li J, Wang J, Li Z, Cai Z, et al. Bone morphogenetic protein 4 inhibits pulmonary fibrosis by modulating cellular senescence and mitophagy in lung fibroblasts. Eur Respir J 2022;60(6):2102307.

[9] Hayek H, Rehbini O, Kosmider B, Brandt T, Chatila W, Marchetti N, et al. The regulation of fatty acid synthase by exosomal miR-143-5p and miR-342-5p in idiopathic pulmonary fibrosis. Am J Respir Cell Mol Biol 2024;70:259–82.
[10] Effendi WI, Nagano T. Connective tissue growth factor in idiopathic pulmonary fibrosis: breaking the bridge. Int J Mol Sci 2022;23(11):6064.
[11] Richeldi L, Fernández Pérez ER, Costabel U, Albera C, Lederer DJ, Flaherty KR, et al. Pamrevlumab, an anti-connective tissue growth factor therapy, for idiopathic pulmonary fibrosis (PRAISE): a phase 2, randomised, double-blind, placebo-controlled trial. Lancet Respir Med 2020;8:25–33.
[12] Leask A. Breathe, breathe in the air: the anti-CCN2 antibody pamrevlumab (FG-3019) completes a successful phase II clinical trial for idiopathic pulmonary fibrosis. J Cell Commun Signal 2019;13:441–2.
[13] Egli M, Manoharan M. Chemistry, structure and function of approved oligonucleotide therapeutics. Nucleic Acids Res 2023;51:2529–73.
[14] Sergeeva OV, Shcherbinina EY, Shomron N, Zatsepin TS. Modulation of RNA splicing by oligonucleotides: mechanisms of action and therapeutic implications. Nucleic Acid Ther 2022;32:123–38.
[15] Crooke ST, Baker BF, Crooke RM, Liang XH. Antisense technology: an overview and prospectus. Nat Rev Drug Discov 2021;20:427–53.
[16] Kulkarni JA, Witzigmann D, Thomson SB, Chen S, Leavitt BR, Cullis PR, et al. The current landscape of nucleic acid therapeutics. Nat Nanotechnol 2021;16:630–43.
[17] Liu F, Xin M, Feng H, Zhang W, Liao Z, Sheng T, et al. Cryo-shocked tumor cells deliver CRISPR-Cas9 for lung cancer regression by synthetic lethality. Sci Adv 2024;10: eadk8264.
[18] Xu X, Kwong CHT, Li J, Wei J, Wang R. Zombie" macrophages for targeted drug delivery to treat acute pneumonia. ACS Appl Mater Interfaces 2023;15:29012–22.
[19] Wu L, Du Z, Li L, Qiao L, Zhang S, Yin X, et al. Camouflaging attenuated Salmonella by cryo-shocked macrophages for tumor-targeted therapy. Sign Transd Target Ther 2024;9:14.
[20] Rinaldi C, Wood MJA. Antisense oligonucleotides: the next frontier for treatment of neurological disorders. Nat Rev Neurol 2018;14:9–21.
[21] Booth BJ, Nourreddine S, Katrekar D, Savva Y, Bose D, Long TJ, et al. RNA editing: expanding the potential of RNA therapeutics. Mol Ther 2023;31:1533–49.
[22] Logtenberg MEW, Scheeren FA, Schumacher TN. The CD47-sirpα immune checkpoint. Immunity 2020;52:742–52.
[23] Gallo J, Kamaly N, Lavdas I, Stevens E, Nguyen QD, Wylezinska-Arridge M, et al. CXCR4-targeted and MMP-responsive iron oxide nanoparticles for enhanced magnetic resonance imaging. Angew Chem Int Ed Engl 2014;53(36):9550–4.
[24] Kassassir H, Papiewska-Pająk I, Kryczka J, Boncela J, Kowalska MA. Platelet-derived microparticles stimulate the invasiveness of colorectal cancer cells via the p38MAPK-MMP-2/MMP-9 axis. Cell Commun Signal 2023;21:51.
[25] Della Latta V, Cecchettini A, Del Ry S, Morales MA. Bleomycin in the setting of lung fibrosis induction: from biological mechanisms to counteractions. Pharmacol Res 2015;97:122–30.
[26] Wind S, Schmid U, Freiwald M, Marzin K, Lotz R, Ebner T, et al. Clinical pharmacokinetics and pharmacodynamics of nintedanib. Clin Pharmacokinet 2019;58:1131–47.
[27] Pan L, Cheng Y, Yang W, Wu X, Zhu H, Hu M, et al. Nintedanib ameliorates bleomycin-induced pulmonary fibrosis, inflammation, apoptosis, and oxidative stress by modulating the PI3K/Akt/mTOR pathway in mice. Inflammation 2023;46:1531–42.
[28] Gao S, Li X, Jiang Q, Liang Q, Zhang F, Li S, et al. PKM2 promotes pulmonary fibrosis by stabilizing TGF-β1 receptor I and enhancing TGF-β1 signaling. Sci Adv 2022;8:eabo0987.
[29] Petersen M, Wengel J. LNA: a versatile tool for therapeutics and genomics. Trends Biotechnol 2003;21:74–81.
[30] Shadid M, Badawi M, Abulrob A. Antisense oligonucleotides: absorption, distribution, metabolism, and excretion. Expert Opin Drug Metab Toxicol 2021;17:1281–92.
[31] Song S, Fu Z, Guan R, Zhao J, Yang P, Li Y, et al. Intracellular hydroxyproline imprinting following resolution of bleomycin-induced pulmonary fibrosis. Eur Respir J 2022;59(5):2100864.